Indian Journal of Chemical Technology
Vol. 28, January 2021, pp. 9-22

Conversion of ethanol to higher alcohols on Ni/M_xO_y-Al_2O_3 (M=La, Ce, Zr, Mg and Ti) catalysts: Influence of support characteristics

Vinayagamoorthi Rathinasamy[1,2], Thirunavukkarasu Kandasamy[2], Krishnamurthy Konda Ramaswamy[2], Viswanathan Balasubramanian[2] & Shanthi Kannan*[,1]

[1]Department of Chemistry, Anna University, Chennai 600 025, India

[2]National Center for Catalysis Research, Indian Institute of Technology, Madras, Chennai 600 036, India

E-mail: shanthiramesh@annauniv.edu.in

Received 6 August 2020; accepted 3 October 2020

A new series of alumina supported nickel (8% w/w) catalysts, modified with promoters, La_2O_3, CeO_2, ZrO_2, MgO and TiO_2, highly active for the conversion of ethanol to butanol and higher alcohols, at 200°C-220°C, in batch mode, under autogenous pressure, has been investigated. XRD and XPS results indicate the presence of metallic Ni and Ni aluminate as the active phases. H_2-TPR studies reveal that the introduction of promoters improves nickel dispersion, reducibility and moderates the metal-support interactions.TPD of ammonia and CO_2 studies establish the strong influence of the promoter oxides on the strength and population of acidic and basic sites. Ethanol conversion at 200°C varies in a narrow range, 36-42%. CeO_2 and MgO modified catalysts display maximum selectivity towards butanol (48%) and higher alcohols, (81% and 75%) in comparison with the catalyst based on pristine alumina (28.9% and 40.5%). While the selectivity for butanol and higher alcohols is governed by the basicity of the catalysts, both metal function and basicity are required to drive ethanol conversion. Moderation of acidity helps in minimizing the formation of ethylene and other gaseous products. Analysis of used catalyst indicates that the structural and active phase characteristics are retained during use.

Keywords: Acidity, Basicity, Butanol, C_{4+} alcohols, Ethanol conversion, Heterogeneous catalysts, High Selectivity, Metal function, Nickel-alumina, Oxide promoters

n-Butanol is considered as the next generation biofuel[1a,b] with several advantages over ethanol, such as, higher energy density, lower volatility and solubility in water and non-corrosive nature[2a,b,c]. Besides, butanol blends well with gasoline and with higher air to fuel ratio, renders more efficient combustion. Currently, butanol is produced from propylene by the Oxo process, which is based on the use of the raw material derived from non-renewable resources, and involves application of high pressure, energy inputs and cost of production and hence lacks sustainability. Though an alternative bio-based fermentation process (ABE process) is in practice, a number of factors, like, low yield of butanol, higher cost of substrates and product recovery and solvent toxicity to the *Clostridium* stains, restrict its application on a larger scale[3]. In this context, conversion of ethanol to butanol and higher alcohols, using the classical Guerbet condensation reaction[4] has emerged as an attractive proposition. Especially with the availability of bio-ethanol in plenty, from various bio-mass resources[5,6], such as, bagasse, rice, wheat straw, stems and leaves of corn, wastepaper and waste wood, processes for its conversion to butanol and other higher alcohols are being explored with keen interest, resulting in the revival of Guerbet alcohol chemistry and catalysts therein. Excellent reviews[7,8], covering various stages of development in the heterogeneous as well as homogeneous catalytic processes for the conversion of ethanol to butanol and higher alcohols, based on the chemistry of Guerbet process, have been published. While the debate on multi-step Guerbet route Vs direct self-condensation of ethanol to butanol continues[9], detailed reviews, on various catalysts systems, thermodynamic aspects and plausible reaction pathways for the formation of major as well as minor products, have also been reported[10a,b,c]. Several types of heterogeneous catalysts, based on MgO, Mg−Al-O mixed oxides, Cu/CeO_2, basic zeolites, hydroxyapatite, solid acid supported Cu, alumina and carbon supported metal catalysts have been explored[10,11]. Different types of supported metal catalysts[12-25] that display significant activity for ethanol conversion towards butanol and higher alcohols formation have been investigated.

The key steps in Guerbet process include: a) dehydrogenation of ethanol to acetaldehyde (ACL),

b) conversion of ACL to crotonaldehyde (CRL) by aldol condensation followed by dehydration c) further hydrogenation of CRL to give butanol[7] . While the initial step involves metal or pair of acidic and basic sites for alcohol dehydrogenation, aldol condensation and dehydration of the enolate species require basic sites and acidic sites respectively. Hydrogenation of CRL via butyraldehyde to butanol proceeds on metal sites. Alumina supported nickel catalysts[12-19], that present the requisite active sites for the above surface transformations, have been explored by several research groups for the conversion of ethanol. Cimino *et al*.[12] have observed that alumina and hydroxyapetite are active for ethanol conversion at lower temperature compared to MgO. Jordison et al.[15] could achieve 55% conversion and 71% selectivity for total higher alcohols at 230°C under autogenous pressure, on 8% Ni on Al_2O_3 support modified with 9% La_2O_3, after 10 hrs on stream period. While Chistyakov *et al*.[19] observed 63.5 % ethanol conversion on Ni-Au-alumina at 275°C and 150 bar pressure, Ghasiaskar and Xu[17] could achieve 35% conversion and 62% butanol selectivity on Ni-alumina catalyst at 250°C and 176 bar pressure in continuous flow mode. Appuzo *et al*.[26a,b] have observed that on Ni or Ru supported on MgO modified alumina support, MgO is dispersed as solid solution in alumina, resulting in increase in basicity and stability and the effective dispersion of Ni/Ru, leading to butanol yields up to 6-8%, with 40-60% ethanol conversion in the temperature range 350-400°C in continuous flow mode. A recent publication[26b] describes the techno-economic analysis of the ethanol conversion process, based on Ni/La_2O_3-Al_2O_3 catalyst, for possible commercial exploitation.

Achieving higher selectivity/yield for butanol and higher carbon number alcohols at higher ethanol conversion under moderate reaction conditions, remains a challenge. The distinguishing feature of the present work is towards improving the conversion and selectivity through modifications in alumina support, brought about by the addition (5% w/w of alumina) of metal oxides, like, La_2O_3, CeO_2, ZrO_2, MgO and TiO_2. Besides tuning the acid-base characteristics of alumina, the modifiers could influence the metal (Ni) dispersion, its electronic state and metal-support interactions and hence activity and selectivity. Such changes brought about by added metal oxides have been studied in detail, using different characterization techniques, like, XRD, temperature programmed reduction (TPR), acidity-basicity by ammonia and CO_2 TPD respectively and XPS. Observed activity and selectivity patterns for ethanol conversion have been correlated with the characteristics of the catalysts with a view to understand the mode of action of the catalysts and design catalysts with improved performance.

Experimental Section

Materials

Pural SB grade pseudo boehmite from M/s SASOL Germany, was used as such. Nickel nitrate hexahydrate ($Ni(NO_3)_2.6H_2O$)(98.0%), Magnesium nitrate hexahydrate ($Mg(NO_3)_2.6H_2O$) (98.5%), (Merck), Lanthanum nitrate hexahydrate ($La(NO_3)_2.6H_2O$) (99.0%), Zirconium oxychloride octahydrate ($ZrOCl_2.8H_2O$) (99.5%) (Sisco Research Laboratories) Cerium nitrate hexahydrate ($Ce(NO_3)_2.6H_2O$) (99.9%), (CDH) and TiO_2 anatase (HOMBIKAT UV100 TiO_2) were used as received, without any further purification. Absolute alcohol (99.9%) from Changshu Hongsheng Fine Chemical Co. Ltd., China, was used as such for carrying out reactions.

Preparation of catalysts

Pural SB grade pseudo boehmite was calcined at 450°C in air for 4 h, to get unmodified gamma alumina support. Known amount of unmodified alumina support was dispersed in 20 mL of DM water with continuous stirring. Required quantity of $La(NO_3)_3.6H_2O$ (to obtain 5% w/w of La_2O_3) was dissolved in the slurry and dispersed again by stirring. The slurry was evaporated to dryness at 80°C in a rotary evaporator, followed by drying in the oven at 120°C for12 h. Lanthana modified alumina was then obtained by calcination of the dried material at 600°C for 12 h in nitrogen atmosphere. Similarly, required quantities of oxide precursors, namely, $Ce(NO_3)_3.6H_2O$, $Mg(NO_3)_2.6H_2O$, $Zr(OCl)_2.6H_2O$ and Hombikat UV grade titania (to obtain 5% w/w loading of CeO_2,MgO, $ZrO_2$and TiO_2 respectively with respect to alumina), were added to the alumina-water slurry, dispersed well, dried and calcined as described earlier, to get modified alumina supports. 8% w/w of Ni as aqueous nickel nitrate hexahydrate solution, was impregnated on to the supports by wet impregnation, dried at 120°C for 12 h and reduced under hydrogen gas flow at 500°C for 12 h to obtain the final catalysts.

Characterization of catalysts

Powder XRD diffraction patterns for the catalysts were recorded using Rigaku Corporation, Japan, Model Miniflex-II X-ray diffractometer, with Cu-Kα

(λ =0.15418 nm) radiation in the 2θ range of 10º to 80º and at a scan rate of 3º/min. Ni crystallite size of the catalysts were calculated by X-ray line broadening analysis, using Debye-Sherrer equation N_2 adsorption and desorption isotherms were measured at 77 K using a Micromeritics ASAP 2020 unit. Surface area of the catalysts were measured by BET method and pore volume and pore size distribution by BJH method.

Temperature programmed reduction (TPR) and temperature programmed desorption (TPD) of ammonia and CO_2 were performed on Chem.BET TPR/TPD Chemisorption Analyzer (Quanta Chrome Instrument, USA) equipped with a thermal conductivity detector. For TPR, the catalysts were calcined in air at 300°C, prior to TPR experiments. 50 mg of calcined catalyst was pre-treated at 300ºC in high purity Ar gas (25 cm^3/min) for 1 h and then cooled to room temperature in Ar flow. The gas was changed to 10 % H_2 in Ar (25 cm^3/min) at room temperature. After the stabilization of the baseline, TPR patterns were recorded from room temperature to 800ºC with a heating rate 10º C/ min. For TPD of ammonia, 50 mg of the sample was pre-treated at 300°C in helium flow of 20 mL/min for 1 hour and cooled to room temperature in helium flow. The sample was saturated with ammonia by passing 10% NH_3 in helium gas over the catalyst for 20 min. After flushing out weakly adsorbed ammonia with helium flow at 373K, the baseline was established. TPD of adsorbed ammonia was then recorded by heating the sample in helium flow up to 650°C with a heating rate of 10°C per min. For TPD of CO_2 similar procedure was adopted using CO_2 as a probe molecule instead of ammonia.

Transmission electron micrographs were recorded using JEOL, Japan, Model 3010 Microscope. Few milligrams of the reduced samples (1-2 mg) were dispersed in a few mL (1-2 mL) of ethanol by ultrasonication for 15 min and a drop of the dispersion was placed on a carbon coated copper grid and allowed to dry in air at room temperature.

X-ray photoelectron spectra of the reduced catalysts were recorded using Omicron Nanotechnology, Oxford Instruments, UK, instrument with Mg K_α radiation. The base pressure of the analysis chamber during the scan was $2*10^{-10}$ millibar. The pass energies for individual scan and survey scan are 20 and 100 eV, respectively. The spectra were recorded with step width of 0.05 eV. The data was processed with the Casa XPS software.

Evaluation of catalysts for ethanol conversion

Reaction was carried in batch mode, using a 100 mL Parr reactor with Model 4848 controller unit (Parr instruments, Chicago, USA). 1.83 g of catalyst was dispersed in 20 g of ethanol. After purging three times with N_2 to remove air, the reactor was filled with nitrogen up to 10kg/cm^2 and sealed. The reaction was carried out under autogenous pressure at 200°C and 220°C for 8 h with an agitator speed of 350 rpm. During the reaction the reactor pressure increased gradually with time and stabilized at 45-50 kg/cm^2 after 4 h. After the completion of 8 h, the reactor was cooled to room temperature and a sample of gaseous products for GC analysis was collected in a sample bulb by controlled depressurization of the reactor. Weight of the liquid product after cooling and depressurization was noted so that mass fractions of liquid and gaseous products could be arrived at. Liquid and gaseous products were analysed by gas chromatography. Details on the analysis of product stream and computation of product stream composition are described in the Electronic Supplementary Information.

Results and Discussions

Characterization of catalysts

X-ray diffraction

X-ray diffractogram for the pristine alumina support as presented in Fig S1 shows all major d-lines characteristic of gamma alumina phase at 2θ = 18.8, 36.8°, 45.8° and 66.8°, which correspond to (013), (111), (400) and (440) planes respectively and match closely with the reported values (JCPDS 46-1131). XRD patterns for Ni supported on pristine and modified alumina supports in reduced state are presented in Fig. 1. Diffractogram for reduced Ni/Al_2O_3 (Fig.1a) displays all major d-lines due to gamma alumina phase and in addition, d-lines at 2θ = 51.3° and 76.1°due to (200) and (220) planes for Ni metal (JCPDS-04-0850). The major d-line due to Ni metal at 2θ= 44.4° (111) is masked by the (400) line due to alumina. Since the intensity of the d-line at 2θ= 76.1 is very weak, the d-line at 2θ =51.3° was used to calculate the crystallite size of nickel for all the catalysts (Table.1). Under the preparation conditions adopted, strong metal-support interaction between Ni and alumina leading to the formation of nickel aluminate is possible[27]. However, the d-lines due to nickel aluminate (at 2θ= 19.1°, 31.4°, 37.0°, 45.0° and 65.5°-JCPDS 10-339) are not discernible from those of alumina support, since both phases are structurally

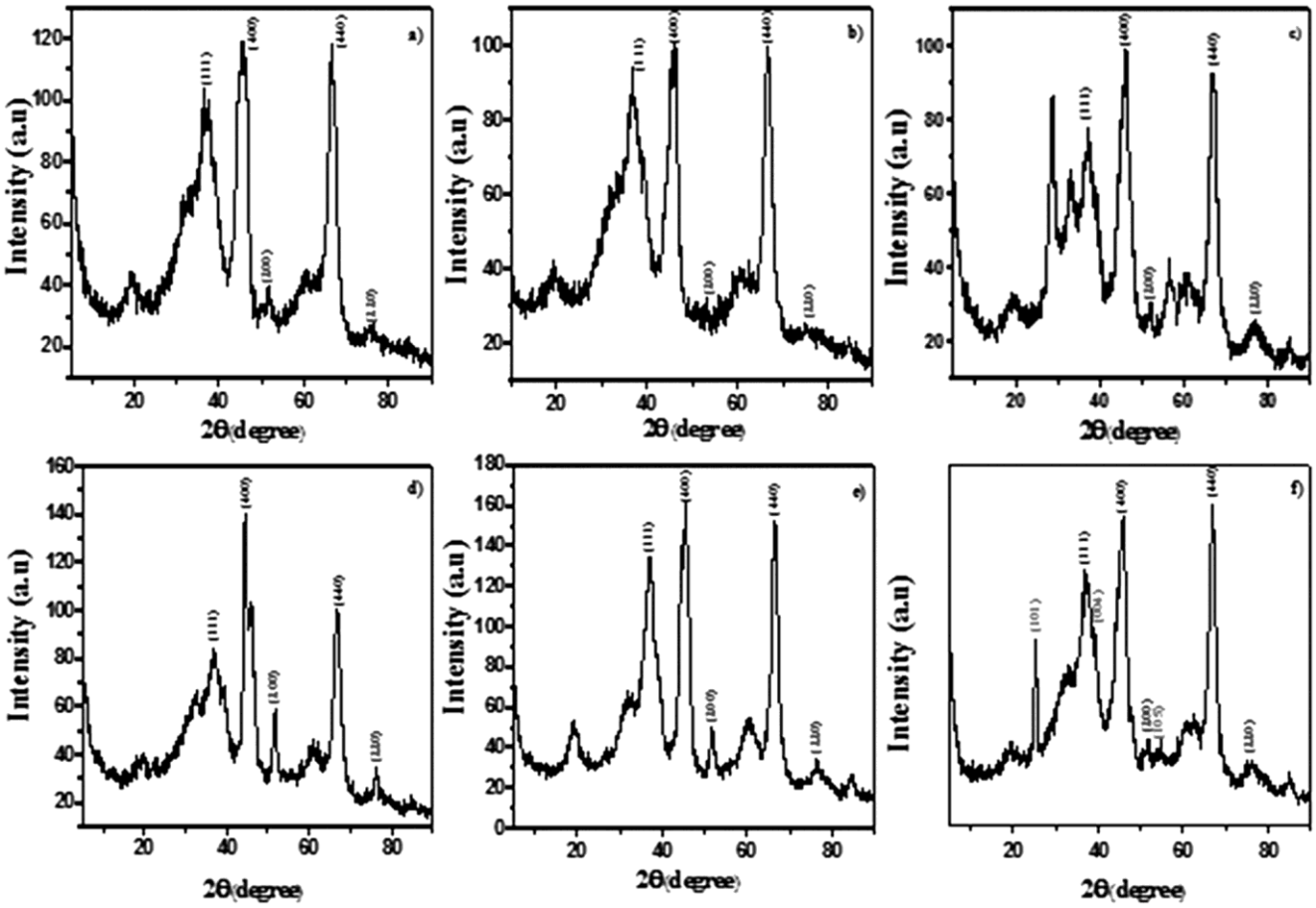

Fig. 1 — X-ray diffractograms for Ni/M_xO_y-Al_2O_3 (M=La, Ce, Zr, Mg &Ti) catalysts: a) 8%Ni/Al_2O_3, b) 8%Ni/5%La_2O_3-Al_2O_3, c) 8%Ni/5%CeO_2 -Al_2O_3, d) 8%Ni/5%ZrO_2-Al_2O_3, e) 8%Ni/5%MgO-Al_2O_3 and f) 8%Ni/5%TiO_2-Al_2O_3

(spinel) similar. 2θ value for (400) plane corresponding to alumina in Ni/Al_2O_3 phase does show a decrease with respect to that for pristine alumina (2θ= 45.4 Vs 45.8) due to the migration and dispersion of Ni into alumina lattice, possibly leading to the formation of surface/bulk nickel aluminate[27,28]. Introduction of Ni and lanthana (Fig.1b) into the alumina phase does not result in any major structural modifications, with very little changes in alumina d-line positions. While no d-lines due to lanthana is observed, indicating its dispersion in alumina lattice [29], the d-lines due to Ni crystallites at 2θ= 53.2° and 75.1°are observed. Ni/CeO_2- Al_2O_3 (Fig.1c) displays major d-lines due to CeO_2 (28.3° (111), 33.1°(211), 56.4º(311), 76.6°(420) (JCPDS 34-03940), besides those for alumina and Ni metal. Major d-lines due to ZrO_2 and MgO (Fig.1 d and Fig.1e) are not distinctly observed in the patterns for Ni/ZrO_2-Al_2O_3 and Ni/MgO-Al_2O_3 possibly indicating that these oxides are well-dispersed on alumina phase, similar to the observations on lanthana modified catalyst. Similarly, in the diffractogram for Ni/TiO_2- Al_2O_3 (Fig.1 f) only one major d-line due to TiO_2 (anatase) at 2θ= 25.2° is observed. Though formation of nickel aluminate phase is possible in all samples, as explained earlier, distinct d-lines are not observed. Crystallite sizes for Ni on pristine and modified alumina supports, calculated by

Table 1 — Textural and structural characteristics of Ni/M_xO_y-Al_2O_3 (M=La, Ce, Zr, Mg &Ti) catalysts

Catalysts	Surface area (m^2/g)	Pore volume (cm^3/g)	Pore diameter (nm)	Crystallite size (nm)
				Ni (200)
Al_2O_3	174	0.44	10.1	
8%Ni/Al_2O_3	136	0.35	10.2	10.8
8%Ni/5%La_2O_3-Al_2O_3	121	0.36	9.6	10.0
8%Ni/5%CeO_2-Al_2O_3	129	0.36	8.6	9.3
8%Ni/5%ZrO_2-Al_2O_3	128	0.33	8.1	9.5
8%Ni/5%MgO-Al_2O_3	118	0.34	9.2	7.4
8%Ni/5%TiO_2-Al_2O_3	114	0.34	9.3	7.6

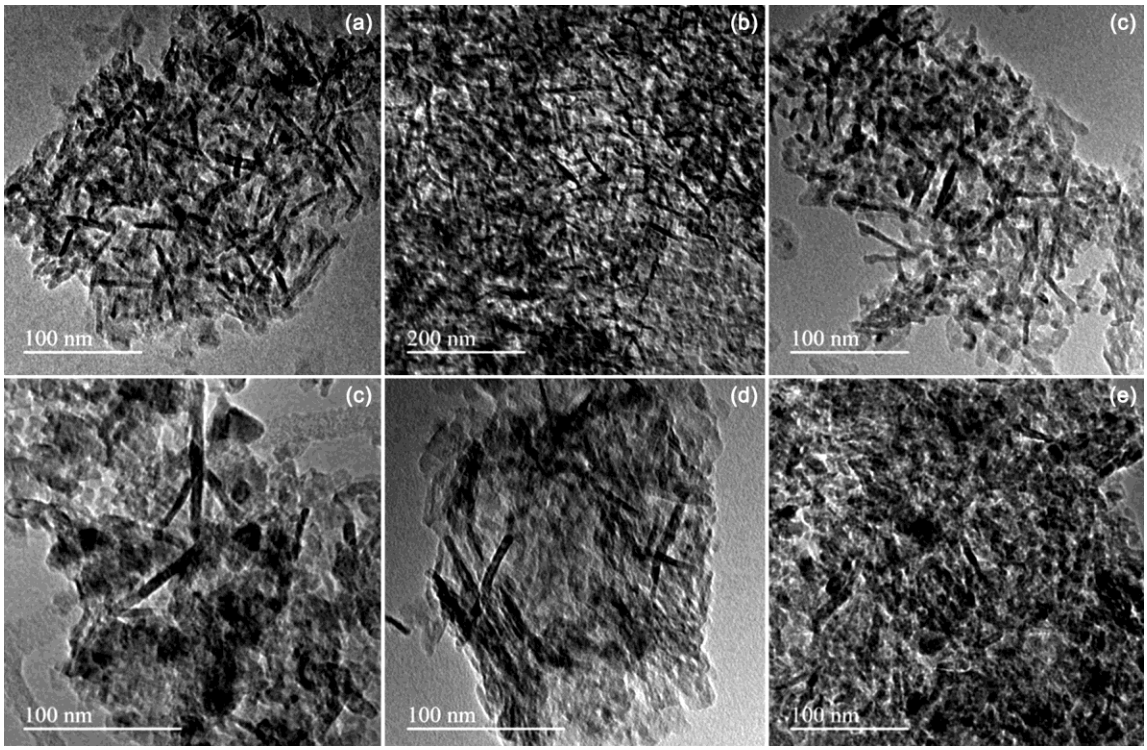

Fig. 2 — TEM micrographs for Ni/M_xO_y-Al_2O_3 (M=La, Ce, Zr, Mg &Ti) catalysts: a) 8%Ni/Al_2O_3, b) 8%Ni-5%La_2O_3/Al_2O_3, c) 8%Ni 5%CeO_2/Al_2O_3, d) 8%Ni-5%ZrO_2/Al_2O_3, e) 8%Ni5%MgO/Al_2O_3 and f) 8%Ni-5%TiO_2/Al_2O_3.

applying the Debye Scherrer equation, are presented in Table.1.

Textural properties

Nitrogen adsorption-desorption isotherms at 77K and pore-size distribution curves according to BJH method for pristine alumina and nickel supported on modified alumina (in reduced state) were obtained and studied. Pristine alumina displays Type IV adsorption-desorption isotherms characteristic of meso porous nature and Type II hysteresis curve, according to de Boer classification, indicating slit shaped pores. Introduction of Ni in alumina brings about perceptible change in surface area and pore volume of pristine alumina (Table. 1). Introduction of nickel and modifiers does not significantly alter the overall pore structure of alumina, but for a modest decrease in surface area, pore volume and mean pore radius.

Transmission Electron Microscopy

Transmission electron micrographs for the reduced catalysts presented in Fig. 2 show fairly good dispersion of nickel crystallites on the supports. All catalysts exhibit needle shaped morphology as reported in literature for alumina supported nickel catalysts [28,30 a,b,c].

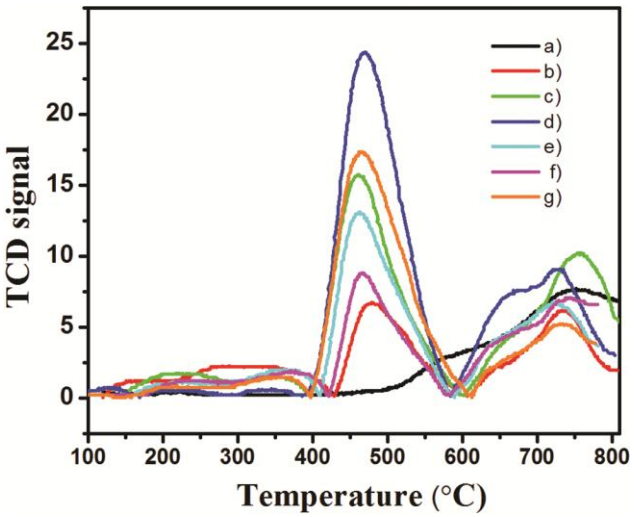

Fig. 3 — H_2 TPR profiles for Ni/M_xO_y-Al_2O_3 (M=La, Ce, Zr, Mg & Ti) catalysts a) Al_2O_3, b) 8%Ni/Al_2O_3, c) 8%Ni/5%La_2O_3-Al_2O_3, d) 8%Ni/5%CeO_2-Al_2O_3, e) 8%Ni/5%ZrO_2-Al_2O_3, f) 8%Ni/5%MgO-Al_2O_3 and g) 8%Ni/5%TiO_2-Al_2O_3

Temperature programmed reduction

TPR patterns for bare alumina support, nickel supported on pristine and modified alumina supported catalysts in calcined state are presented in Fig. 3. In order to study the presence of various reducible species, TPR profiles have been deconvoluted.

Depending on the nickel precursor and loading, the method of incorporation and pre- treatment/reduction procedures adopted, several states of reducible nickel phases have been observed [31]. Further changes in the nature of the supports, like modifications by added metal oxides, namely, La_2O_3, CeO_2, MgO, ZrO_2 and TiO_2 are reflected in terms changes in overall reducibility, nickel dispersion and degree of metal-support interactions in modified supports. In the present work, based on the data from literature[31], three major reduction zones could be identified, in all the six catalysts, with characteristic reduction temperature ranges. Reduction maxima observed in the temperature range 100-400°C (Zone-1) are due to free or weakly bound nickel oxide, those in the temperature range 400-600°C (Zone-2) due to dispersed nickel oxide that exists in the form of solid solution in alumina matrix and the reducible phases in the temperature range 600-800°C (Zone-3) due to surface and bulk nickel aluminate formed by strong interaction with support.

As shown in Fig. 3, amongst the catalysts, Ni supported on pristine alumina displays relatively minimum reducibility as indicated by hydrogen consumption. All Ni catalysts supported on modified alumina are characterized by higher reducibility, in the following order:Ni/ CeO_2-Al_2O_3> Ni/ TiO_2-Al_2O_3>Ni/ La_2O_3-Al_2O_3>Ni/ ZrO_2-Al_2O_3>Ni/ MgO-Al_2O_3 Presence of Ni in metallic state is essential for the dehydrogenation-hydrogenation steps during ethanol conversion process and this aspect would be discussed in the following section. A compilation of TPR maxima in the three reduction zones and the corresponding hydrogen consumption (as % of total consumption) are given in Table. 2. While these three distinct reduction zones (zones 1-3) are observed in all the six catalysts (Table.2), the relative proportions of the reducible phases within the catalysts differ with respect to the nature of modified supports. In the case of nickel supported on pristine alumina, based on hydrogen consumption, it is observed that the proportions of free or weakly bound nickel oxide (zone-1) and nickel oxide involved in the formation of surface/bulk nickel aluminate (zone-3), are larger compared to those on modified supports (Table 2). Addition of lanthana (Fig.S3b) increases the proportion of dispersed NiO at the expense of free NiO and NiO involved in surface/bulk nickel aluminate formation and overall reducibility of Ni^{2+} increases, which is in line with the literature reports[27,28]. With respect to the maxima (479°C) observed for NiO in dispersed state in Ni-Al_2O_3, the corresponding maxima for all the modified alumina catalysts are shifted to lower temperatures (461-470°C) (Table 2) indicating ease of reduction and increase in overall reducibility, as revealed by increase in hydrogen consumption (42.2 to 86%) in Zone-2. Especially in the case of Ni/CeO_2 Al_2O_3, the redox pair Ce^{3+}/Ce^{4+} is expected to facilitate the reduction of Ni^{2+}[32,33] and accordingly maximum overall reducibility is observed in this case (Fig.2d). Thus, the modifiers improve Ni dispersion, reducibility and modulate the nickel-support (alumina/ modified alumina) interactions and hence the characteristics of active phases.

X–ray Photoelectron Spectroscopy

XPS binding energy data for all the catalysts in reduced state have been presented in Table 3. XPS profiles for Ni core electron states in pristine and modified alumina supports are given in Fig.4 and those for modifier oxides in Fig.S4. Deconvolution of $Ni2p_{3/2}$ line for Ni supported on pristine alumina reveals two maxima, at 853.3 eV and 856.8 eV (Fig. 4a). With respect to the reported binding energy (BE) value of 852.6 eV[34a,b] for clean Ni metal, the binding energy value for Ni dispersed on Al_2O_3 is on the higher side (+0.7eV), revealing that Ni is in as electron deficient state. The other component of the $2p_{3/2}$ peak at 856.8 eV is attributed to Ni $2p_{3/2}$ in nickel aluminate[35]. In the case of Ni/La_2O_3-Al_2O_3 (Fig.4b) the peak at 835.4 eV is attributed to La $3d_{5/2}$ for lanthana which is followed by its satellite peak at 838.3 eV [36].

Table 2 — Temperature programmed reduction characteristics of Ni/M_xO_y-Al_2O_3 (M=La, Ce, Zr, Mg & Ti) catalysts

Catalysts	TPR maxima (°C) (Hydrogen consumption (%))		
	Zone-I (100°C-400°C)	Zone-II (400°C-600°C)	Zone-III (600°C-800°C)
8%Ni/Al_2O_3	157, 278, 374 (22.8)	479 (42.2)	660, 735 (34.9)
8%Ni/5%La_2O_3-Al_2O_3	219, 355 (6.3)	461 (65.3)	662,756 (28.3)
8%Ni/5%CeO_2-Al_2O_3	175, 302 (7.4)	470 (70.2)	658, 730 (22.3)
8%Ni/5%ZrO_2-Al_2O_3	217, 359 (8.1)	462 (69.2)	649, 717 (22.5)
8%Ni/5%MgO-Al_2O_3	237, 371 (9.6)	467 (81.8)	648, 726 (8.5)
8%Ni/5%TiO_2-Al_2O_3	229, 356 (4.8)	469 (86.0)	646, 722 (9.1)

Table 3 — XPS Binding energies (eV) for core electrons for reduced Ni/M_xO_y-Al_2O_3 M=La, Ce, Zr, Mg and Ti) catalysts

Catalysts	Al_{2p} (eV)	Ni_{2p} (eV)	La_{3d} 5/2 3/2	Ce_{3d} (eV)	Zr_{3d} (eV)	Mg_{2p} (eV)	Ti_{2p} (eV)
8% Ni/Al_2O_3	74.1	853.3 856.8	-	-	-	-	-
8% Ni/5% La_2O_3-Al_2O_3	73.6	853.1 856.5	835.4, 851.9 838.2, 855.0	-	-	-	-
8% Ni/5% CeO_2-Al_2O_3	73.3	853.0 856.0	-	886.0 889.6	-	-	-
8% Ni/5% ZrO_2-Al_2O_3	74.2	853.8 856.9	-	-	185.4 182.9	-	-
8% Ni/5% MgO-Al_2O_3	74.1	853.3 856.6	-	-	-	50.1	-
8% Ni/5% TiO_2-Al_2O_3	76.5	852.1 858.1	-	-	-	-	456.9 462.3

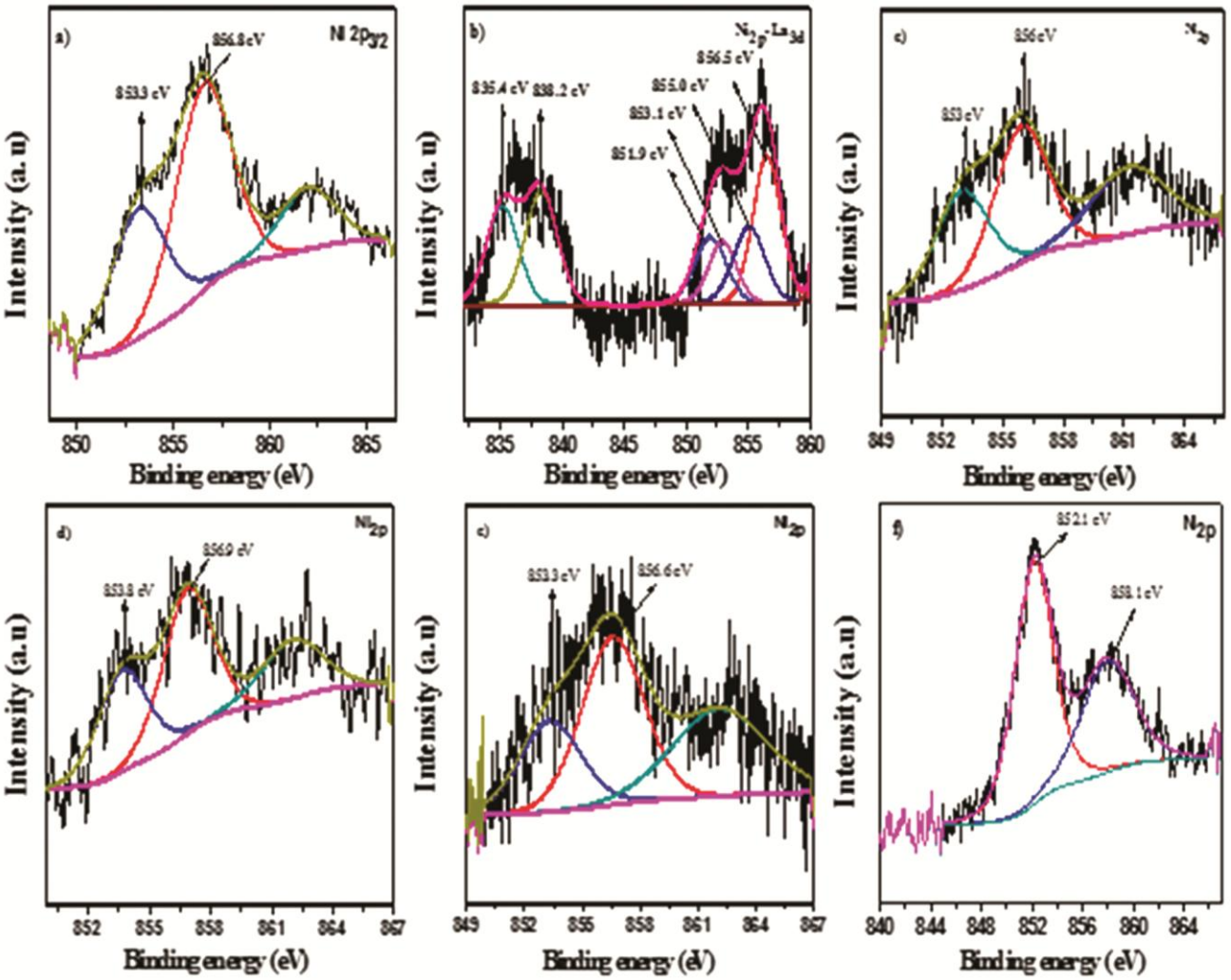

Fig. 4 — XPS profiles for Ni supported on pristine and modified alumina supports a) $8\%Ni/Al_2O_3$, b) $8\%Ni\text{-}5\%La_2O_3/Al_2O_3$, c) $8\%Ni\text{-}5\%CeO_2/Al_2O_3$, d) $8\%Ni\text{-}5\%ZrO_2/Al_2O_3$ e) $8\%Ni5\%MgO/Al_2O_3$ and f) $8\%Ni\text{-}5\%TiO_2/Al_2O_3$

The observed BE of 835.4 eV for La $3d_{5/2}$ is higher than the reported values for La_2O_3 (833.2 eV) and $LaAlO_3$ (833.8) [36] and is very close to the values of BE 835.0 eV[37] and 835.8 eV[38] reported for La dispersed in alumina phase. XPS profile in the region 850-860 eV is resolved into four peaks. The first pair at 851.9 eV and 853.1eV is due to La$3d_{3/2}$ for lanthana[36] and Ni $2p_{3/2}$ for Ni metal. In the second pair, the peak

at 855 eV is the satellite peak for $La3d_{3/2}$ and the one at 856.8 eV is the line for Ni $2p_{3/2}$ in nickel aluminate. XPS lines due to $Ce^{4+}3d_{3/2}$ core level are reported at 900.8 eV, 907.2 eV and 916.7 eV and $3d_{5/2}$ core levels at 882.4 eV, 888.8 eV and 898.1 eV [39-42.].Corresponding XPS lines for Ce^{3+} are expected at 903.7 eV, 884.7 eV, 899.2 eVand 880.1 eV [39,42,43]. In the present work, only two prominent XPS lines at 886 eV and 889.6 eV are observed for Ce, which could be assigned to Ce^{3+}(884.7 eV) and Ce^{4+}(888.8 eV), possibly indicating the presence of both oxidation states. ZrO_2, MgO and TiO_2 modified catalysts (Figs. 4 c, d and e) also display peaks at 853.8 eV and 853.3 eV and 852.1 eV due to Ni $2p_{3/2}$ for Ni metal and at 856.9 eV and 856.6 eV and 858.1 eV due to Ni $2p_{3/2}$ in nickel aluminate respectively. In the case of other modifier oxides, XPS line at 182.9 eV and 185.4 observed for $Zr3d_{5/2}$ $Zr3d_{3/2}$ are close to the reported[44] binding energy values of 182.75 eV and 185.14 eV respectively. Similarly, the observed core level binding energy values of 50.1 eV for Mg2p and 456.9 eV and 462.3 eV for Ti2p are close to the respective reported values[36.45]. Al 2p profiles for La & Ce modified alumina display shift towards lower BE values at 73.6 eV and 73.3 eVrespectively with respect to the corresponding XPS line for unmodified alumina at 74.2 eV. Such shift in BE is attributed to a strong interaction between Ni and surface Al ions[46]. While no significant change in Al2p BE values are observed in ZrO_2 and MgO modified alumina, BE for TiO_2 modified alumina shifts to higher side. Modifiers thus influence the electronic state of the alumina phase.

Acidity and basicity measurements

Distribution of acid sites, as revealed by temperature programmed desorption profiles for ammonia (Fig. S5) for all the catalysts in the reduced state, is given in Table 4.

Weak (200-300°C), medium (300-400°C) and strong (400-500°C) acid sites are observed in all the catalysts. Ni supported on pristine alumina displays maximum total acidity and acid sites density. While addition of lanthana and ceria to Ni/Al_2O_3 brings about reduction in total acidity and acid site density, the reduction is substantial with the supports modified by other three additives, ZrO_2, MgO and TiO_2. Moderation of overall acidity of alumina by addition of La_2O_3, CeO_2, ZrO_2 and MgO has been reported by Sánchez-Sánchez *et al*[31]. Attenuation of acidity and increase in basicity of lanthana and ceria modified alumina have been observed by Garbarino *et al*.[47] and Vazquez *et al*.[48].

Distribution of basic sites, compiled on a similar basis, for all the catalysts in reduced state, is presented in Table 5. Corresponding CO^2 desorption profiles are presented in Fig.S6 Weak. (100-200°C), medium (200-300°C) and strong (300-500) basic sites are observed in all the catalysts. All catalysts based on modified alumina support display higher basicity and basic site density when compared to the catalyst supported on pristine alumina.

The observed CO_2 TPD maxima for ceria modified catalyst (with characteristic desorption maxima at 199, 355 & 485°C) indicate the presence of relatively stronger basic sites, though the total basicity is less. Vazquez *et al*.[48] could distinguish the nature of basic sites in La_2O_3-$Al_2O_3$and CeO_2-Al_2O_3 using conversion of isopropanol as the probe reaction. While on La_2O_3-Al_2O_3 only propene is observed, on CeO_2-Al_2O_3 propene and acetone are observed as products, indicating the presence of strong basic sites responsible for dehydrogenation.

Results observed the present work on Ni/CeO_2-Al_2O_3 are in line with the observations reported by Vazquez et

Table 4 — Distribution of acid sites by ammonia TPD for Ni/M_xO_y-Al_2O_3 (M=La, Ce, Zr, Mg &Ti) catalysts

Catalysts	Distribution of acid sites				
	Weak °C/mmol/g	Medium °C/mmol/g	Strong °C/mmol/g	Total mmol/g	Acid site Density µmol/m^2
8%Ni/Al_2O_3	283	385	474	2.38	17.5
	0.53	1.32	0.53		
8%Ni/5%La_2O_3-Al_2O_3	279	399	483	1.88	15.5
	0.47	1.01	0.40		
8%Ni/5%CeO_2-Al_2O_3	267	370	461	1.67	12.9
	0.53	0.93	0.21		
8%Ni/5%ZrO_2-Al_2O_3	221	352	451	1.52	11.9
	0.25	0.75	0.52		
8%Ni/5%MgO-Al_2O_3	229	356	455	1.19	10.1
	0.2	0.6	0.39		
8%Ni/5%TiO_2-Al_2O_3	211	398	482	1.06	9.3
	0.35	0.52	0.19		

Table 5 — Distribution of basic sites by CO_2 TPD for Ni/M_xO_y-Al_2O_3 (M=La, Ce, Zr, Mg and Ti) catalysts

Catalysts	Distribution of basic sites				
	Weak °C/mmol/g	Medium °C/mmol/g	Strong °C/mmol/g	Total mmol/g	Basic site Density µmol/m^2
8%Ni/Al_2O_3	130	251	313	0.102	0.75
	0.025	0.046	0.031		
8%Ni/5%La_2O_3-Al_2O_3	128	274	358	0.392	3.2
	0.049	0.183	0.16		
8%Ni/5%CeO_2-Al_2O_3	199	355	485	0.165	1.3
	0.019	0.132	0.014		
8%Ni/5%ZrO_2-Al_2O_3	141	288	407	0.302	2.3
	0.019	0.215	0.068		
8%Ni/5%MgO-Al_2O_3	143	275	386	0.397	3.4
	0.035	0.174	0.188		
8%Ni/5%TiO_2-Al_2O_3	128	269	337	0.089	2.3
	0.019	0.049	0.021		

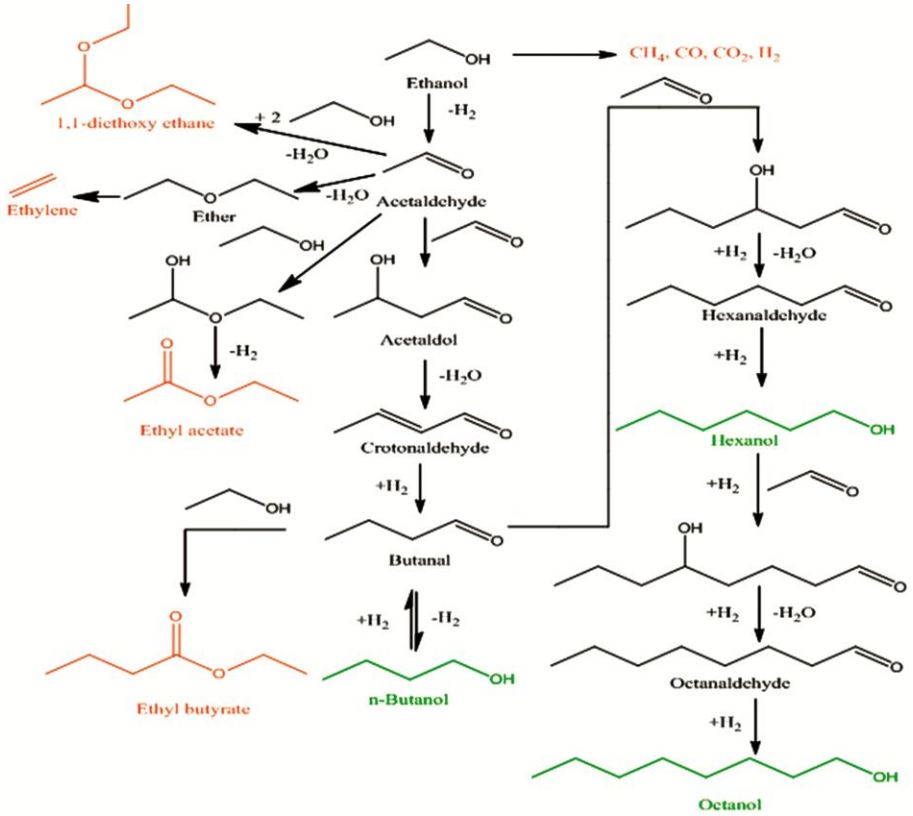

Scheme 1 — Possible transformations of ethanol and acetaldehyde on Ni/M_xO_y-Al_2O_3 (M=La, Ce, Zr, Mg and Ti) catalysts

al[48].In general, all catalysts with modified alumina supports, display relatively higher population of medium strength acidic/basic sites, which could influence the reaction pathways in ethanol condensation process. These aspects are discussed in the following section.

Conversion of ethanol to higher carbon number alcohols

Though the reaction has been carried out at 200°C and 220°C, for a complete understanding and analyses of ethanol conversion, product distribution and selectivity, the data at 200°C are considered.

Product distribution

Complete distribution of products, after 8 hrs of reaction at 200°C on all catalysts, is presented in Table S2. Besides unconverted ethanol, butanol, hexanol, octanol and ethylene are observed as the major products along with more than 20 minor products. Presence of small amounts of aldehydes, namely, acetaldehyde, crotonaldehyde and butyraldehyde, in the product streams from all catalysts, indicate that the process proceeds through the classical Guerbet reaction pathway. Scheme 1 presents possible transformations of

ethanol and acetaldehyde, the primary product in the process. Pathways for the formation of the desired products (butanol, hexanol and octanol) and minor products from acetaldehyde are illustrated in Scheme 1. Since the catalysts contain acidic and basic sites of different nature, strength and population, (Tables 4 and 5), ethanol and acetaldehyde undergo a range of transformations, resulting in the formation a number of minor products, which are grouped into:

i) Ether, ethyl acetate and acetal,
ii) C_3-C_4 aldehydes (acetaldehyde, crotonaldehyde and butyraldehyde),
iii) C_{4+}esters, aldehydes and ketones
iv) C_1 –C_5 gaseous hydrocarbon products (including ethylene, CO and CO_2).

Trends in the formation of the products (mole%) on the six catalysts are presented in Fig. 5a-5e.

Correlations on the product formation with inherent acidity-basicity of the catalysts are presented in Fig.6a to 6c. Formation of di-ethyl ether and ethyl acetate in small amounts (Fig. 5a) is due to inherent acidity of the catalysts. It is likely that the presence of relatively higher acidity on $Ni/Al_2O_3$and Ni/La_2O_3-Al_2O_3 catalysts (Table 4) promotes further dehydration of ether to ethylene and hence ether is not observed on these catalysts. Relatively higher amounts of C_3-C_4 aldehydes in $Ni/Al_2O_3$and Ni/La_2O_3-Al_2O_3 catalysts (Fig. 5b) compared to other four catalysts indicate that aldol condensation of acetaldehyde is slower on these two catalysts and is facilitated on the later group of catalysts due to higher basicity (Table 4). Higher basicity entails faster aldehyde condensation/ consumption. Besides, hydrogenation of crotonaldehyde and butyraldehyde are also favoured on these four catalysts due to higher reducibility/metallic nickel (Fig.2). On similar grounds, higher amounts of C_{4+}esters and ketones are observed on lanthana, ceria, magnesia and zirconia modified catalysts(Fig.5c), due to relatively higher basicity and consequent facile aldol condensation.Young et al.[48] have observed that aldol condensation on titania is inhibited in presence of ethanol due to competitive adsorption. Hence formation of C_{4+}esters and ketones via aldol condensation is less on titania modified catalyst. Ni/Al_2O_3 has the lowest basicity.

Ethylene in significant amounts is formed (Fig. 5d) due to acid catalyzed conversion of ethanol to di-ethyl ether, followed by dehydration (Scheme 1). Fig. 6a shows a direct relationship between the total acidity of the catalysts and mole % ethylene. Higher ethylene formation observed on Ni/TiO_2-Al_2O_3, in spite of having lowest total acidity, is due to the presence of

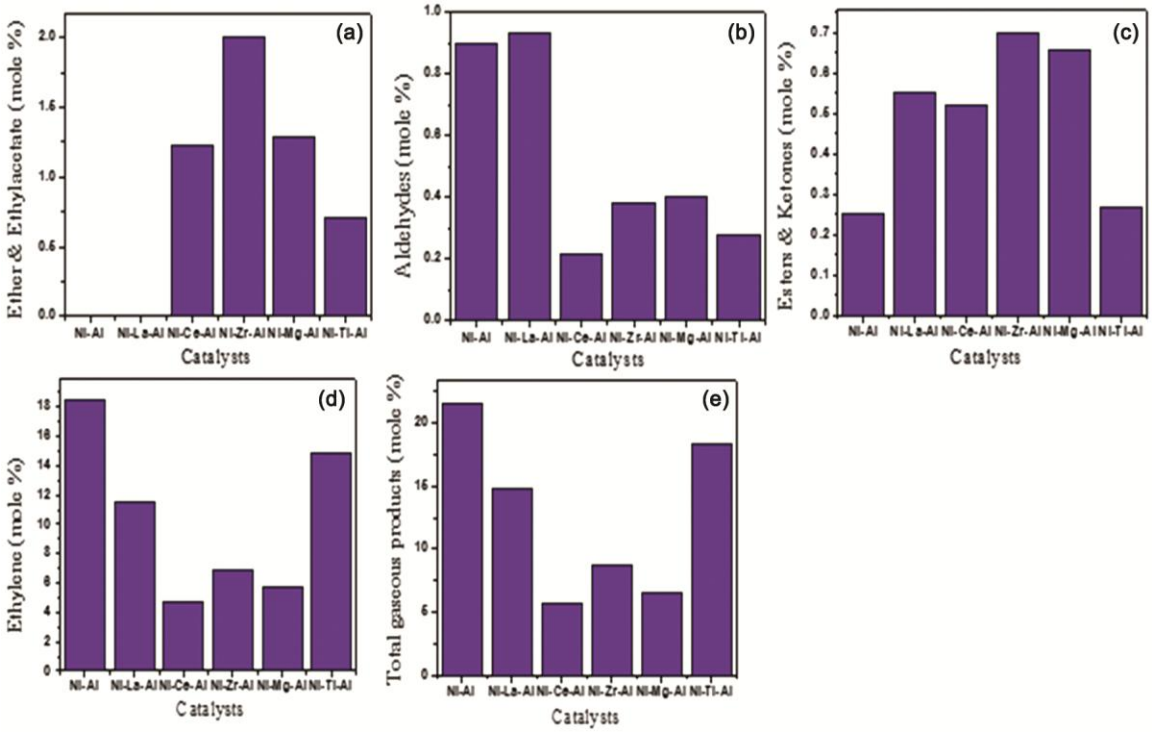

Fig. 5 — Trends in the formation of minor products during ethanol conversion on Ni/M_xO_y-Al_2O_3 (M=La, Ce, Zr, Mg &Ti) catalysts a) Ether and ethyl acetate b) C_3-C_4Aldehydes c) C_{4+}Esters andketones d) Ethylene and e) C_1-C_5 gaseous hydrocarbons

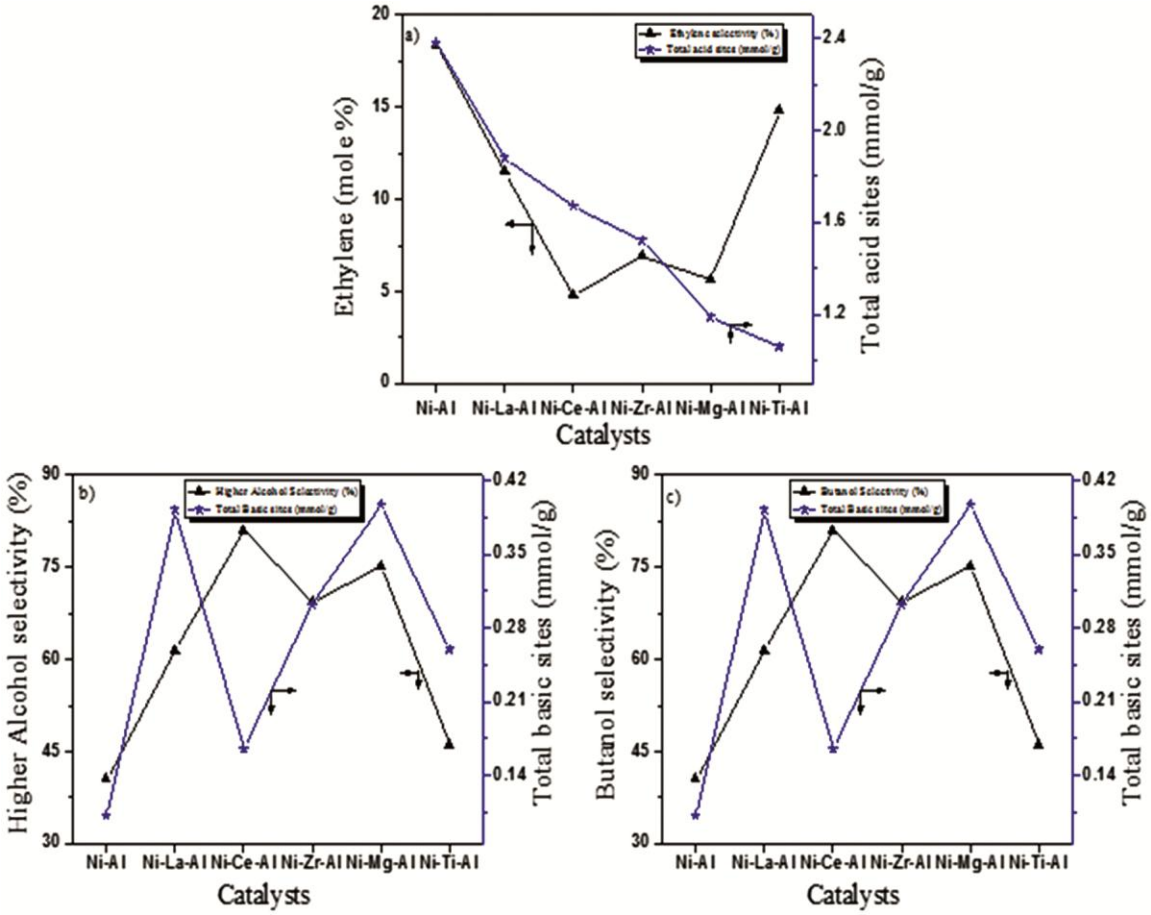

Fig. 6 — Correlations between a) Total acid sites and ethylene selectivity b) Total basic sites and higher alcohol selectivity and c) Total basic sites and butanol selectivity

strong acid sites with a characteristic desorption maximum at 482°C (Table 4).Young *et al.*[48] observed that titania is highly acidic and converts ethanol to diethyl ether. Similarly, Ni/La_2O_3-Al_2O_3 with strong acid sites (desorption maximum at 483°C, Table 4) also displays higher ethylene formation compared to other catalysts, wherein lower acidity levels lead to a decrease in ethylene formation. Thus, besides total acidity, strength of the acid sites is observed to be a crucial parameter. Similar correlation is observed between C_1-C_5 hydrocarbons formation and acidity as well (Fig. 5e).

Conversion of ethanol

Conversion of ethanol and selectivity for butanol and higher alcohols at 200°C and 220°C are presented graphically in Fig. 7. With respect ethanol conversion of 38.2% on Ni catalyst supported on pristine alumina, moderate increase in conversion at 200°C is observed on Ni/La_2O_3-Al_2O_3 (42.3%) and Ni/CeO_2-Al_2O_3 (41.1%) catalysts. While Ni/MgO-Al_2O_3 and Ni/TiO_2-Al_2O_3 display slightly lower ethanol conversion (36.2%), no change in ethanol conversion

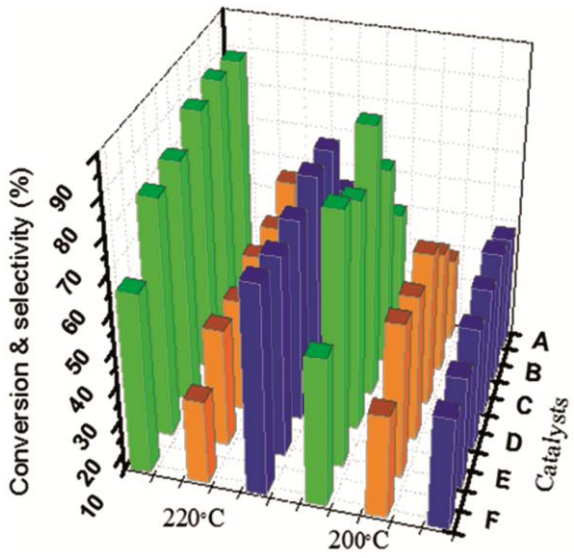

Fig. 7 — Ethanol conversion( ), higher alcohol ( ) and butanol selectivity ( ) on Ni/M_xO_y-Al_2O_3 (M=La, Ce, Zr, Mg &Ti) catalysts at 200°C and 220°C, A) Ni/Al_2O_3, B) $Ni/5\%La_2O_3$-Al_2O_3, C) $Ni/5\%CeO_2$-Al_2O_3, D) $Ni/5\%ZrO_2$-Al_2O_3, E) $Ni/5\%MgO$-Al_2O_3 and F) $Ni/5\%TiO_2$-Al_2O_3

is observed on Ni/ ZrO_2 -Al_2O_3 vis-a-vis Ni/Al_2O_3. Both lanthana and ceria modified catalysts display higher reducibility, especially of dispersed NiO, resulting in metallic Ni, responsible for initial and final steps in the ethanol conversion process, namely dehydrogenation of ethanol and hydrogenation of crotonaldehyde/ butyraldehyde. On the contrary, reducibility of MgO and ZrO_2 modified catalysts only slightly higher than that for the base catalyst, Ni/Al_2O_3. Though titania modified catalysts displays high reducibility, ethanol conversion is lower, since the second major step, aldol condensation of acetone, is retarded due to competitive adsorption of ethanol[48]. Moderate improvement in ethanol conversion observed for lanthana and ceria modified catalysts could be ascribed to improvements in reducibility. Jordison et al.[15] also observed moderate improvement on ethanol conversion on lanthana (55%) and ceria (50%) modified Ni/Al_2O_3 catalysts compared to the unmodified catalyst (46%) but at higher temperature, 230°C and after 10 hrs of reaction.In comparison with ethanol conversion values reported earlier on alumina supported nickel catalysts (Table S1), higher conversions at lower pressure and temperature are realized in the present work.

XRD and XPS results reveal the presence of both Ni metal and nickel aluminate phases in reduced catalysts. Since all the catalysts are reduced in hydrogen at 500°C, based on the TPR profiles Fig. 2 for calcined catalysts, it is inferred that the highly dispersed NiO is reduced to nickel metal, which act as active sites for the dehydrogenation of ethanol to acetaldehyde. Ni^{2+} in nickel aluminate act as Lewis acid sites. Presence of acetaldehyde in particular, in the product streams of all catalysts, indicates that the rate of initial/primary aldol condensation of acetaldehyde, which is considered as the rate determining step[15,49], needs to be further enhanced to improve conversion. As ethanol conversion increases, the concentration of secondary aldehydes builds up, which compete with primary aldehydes for the basic sites required for aldol condensation. Hence, only a marginal increase in ethanol conversion is observed, though ethanol dehydrogenation step is accelerated by Ni metal. Increasing the loading of basic oxides like ceria may lead to further improvement of the acetaldehyde condensation rate and hence ethanol conversion. Improving hydrogenation function by addition of a second metal could help to increase rate of hydrogenation of secondary aldehydes (crotonaldehyde, butyraldehyde etc.,) which in turn increase ethanol conversion.

These two aspects, namely, increasing the loading of ceria and exploring addition of second metal to Ni are currently under investigation. According to Cimino *et al*[12] alumina is active for ethanol conversion at a lower temperature compared to magnesia. Young et al[48] in their studies on ethanol conversion and aldol condensation on TiO_2, hydoxyapetite (HAP) and MgO have observed that the activity for aldol condensation follows the order TiO_2> HAP >>MgO. Besides, on titania, aldol condensation rate is inhibited in presence of ethanol due to competitive adsorption, while it is not so with MgO and HAP. Such inherent variations in the characteristics of the promoter oxides could affect overall conversion of ethanol on nickel catalysts with modified supports. At 220°C ethanol conversion increases to 61 to 65% with modified catalysts compared to 45.5 % with unmodified one.

Selectivity towards butanol and higher alcohols

In contrast to the moderate improvement in ethanol conversion, substantial increase in selectivity for butanol (BLS) and higher alcohols (HAS) is observed (Fig 6b, 6c) with catalysts based on modified supports. Ceria and magnesia modified catalysts display HAS of 81% and 75% respectively and 48% for BLS. Lanthana and zirconia modified catalysts also exhibit significant increase in selectivity for HAS and BLS compared to Ni catalyst supported on pristine alumina. Observed increase in selectivity for HAS and BLS are related to the increase in the basicity of catalysts with modified supports (Table 5, Fig.6b and 6c). Increase in the basicity essentially increases the rate of aldol condensation of aldehydes, which leads to the formation of butanol and higher alcohols. Though total basicity of Ni/Ce_2O_3-Al_2O_3 catalyst is the lower, the presence of strong basic sitesin comparison with other catalysts, with characteristic desorption maxima at relatively higher temperatures, 199, 355 and 485°C (Table 5), could be responsible for higher butanol and C_{4+} alcohols selectivity. Jian *et al*.[50] have attributed high butanol selectivity (55%) and yield (21.6%) observed on Cu-Ce/AC catalysts to high basicity of CeO_2 which promotes aldol condensation. Similarly, MgO and ZrO_2 modified catalysts with CO_2desorption maxima at higher temperatures, 386°C and 407°C respectively (Table 5), also display higher butanol and C_{4+}alcohols selectivity. Both strength and the population of basic sites are needed to achieve selectivity for higher alcohols.

Though substantial increase in ethanol conversion is observed at 220°C, the selectivity for butanol decreases from 45-48% at 200°C (with ceria, zirconia and magnesia modified catalysts) to 36-40% at higher temperature, possibly due to the conversion to higher alcohols and gaseous products. XRD, TEM and XPS data for a typical used catalyst show that the structural integrity and active phase characteristics are retained.

Role of acidic and basic sites in the ethanol conversion process has been studied by several researchers[7,10,12,15,16,18,20,22,23,26a] on different active phase/support systems and have been largely qualitative. A systematic study undertaken in the present work on the influence of support characteristics reveals simultaneous changes in the characteristics of the catalysts, like, reducibility of Ni^{2+}, Ni metal dispersion, metal-support interaction and its electronic state besides acidity and basicity and clearly brings out property-performance correlations. While the selectivity for butanol and higher alcohols is governed by the basicity, both metal function and basicity are required to drive ethanol conversion. Moderation of acidity, on the other hand, helps in the minimization of ethylene and other gaseous products.

Recent studies by Benito *et al.*[51] on Cu-hydrotalcite derived catalysts reveal slightly higher butanol selectivity (52.1%) but at lower conversion (32.1%), higher temperature (230ºC) and after 12 h of reaction. Wang et al.[52] have reported 19.1% yield of butanol at 50.1% ethanol conversion after 8 h at 275ºC and 2MPa pressure, but the catalyst undergoes phase transformation to $Ca(OH)_2$ during reaction. Studies have been extended to bi-metallic catalysts based on Au[54] and three component Cu-Ni-Mn catalysts[53] as well, at higher temperatures and pressures. Though these studies are in the right direction, ethanol conversion and butanol/higher alcohols selectivity are not attractive. Balancing the dehydrogenation-hydrogenation functions and moderation of acidity-basicity (nature, strength and population of sites) to prevent the formation of numerous side products are the key aspects that need further investigation.

Conclusion

A new series of nickel (8% w/w of alumina) supported on alumina catalysts with the general formula Ni/M_xO_y-Al_2O_3 (M=La, Ce, Zr, Mg and Ti, with 5% w/w M_xO_y) has been evaluated for the conversion of ethanol to butanol and higher alcohols in batch mode. Presence of small amounts acetaldehyde, butanal and crotonaldehyde in the product pattern indicates that the process follows the Guerbet reaction pathway. Introduction of promoter oxides influences nickel metal dispersion, reducibility, metal support interactions and hence the electronic character of the active phase consisting of nickel metal and nickel aluminate. Besides, acid-base characteristics, ie., nature, strength and population of sites, also vary with respect to the promoter oxides. While ethanol conversion is governed by the metal function and basicity, selectivity for butanol and higher alcohols is influenced by the basicity of the catalysts. Moderation of acidity by the promoters retards the formation of ethylene and other C_1-C_5 hydrocarbon products. Increasing basicity of the catalysts with higher loading of ceria, improving metal function by addition of second metal with Ni and optimization of acidity-basicity to minimize side products formation are the useful strategies for achieving higher ethanol conversion activity and selectivity for butanol and higher alcohols.

Conflicts of interest

There is no conflict of interests among the authors

Acknowledgements

The authors gratefully acknowledge Department of Science and Technology, GoI, New Delhi, for providing the all facilities for research in Catalysis at NCCR, IIT Madras, Chennai and adequate instrumentation facilities for characterization of catalysts in the Department of Chemistry, Anna University, Chennai, and M/s Nagarjuna Fertilizers & Chemicals Ltd. Hyderabad, India, for a project grant.

References

1 (a) Harvey B G & Meylemans H A, *J Chem Technol Biotechnol*, 86 (2011) 2; (b) Xue C, Zhao X Q, Liu C G, Chen L J & Bai F W, *Biotechnol*, Adv, 31 (2013) 1575.
2 (a) Thompson R, Behnam M, Swana J & Yang Y, *Bioresour*, Technol, 102 (2011) 2112; (b) Singh S B, Dhar A & Agarwal A K, *Renewable Energy*, 76 (2015) 706; (c) Derre P, *Biotechnol J*, 2 (2007) 1525. Ndaba B, Chiyanzu I & Marx S, *Biotechnology Reports*, 8 (2015) 1.
3 (a) Derre P & Ann N Y, *Acad Sci*, 1125 (2008) 353; (b) Bankar S B, Survase S A, Ojamo H & Granstrçm T, *RSC Adv*, 3 (2013) 24734.
4 Guerbet M C, Comptesrendus de l, *Académie des Sci*, 149 (1909) 129.
5 Cunha M, Roman A, Carvalho M & Domingues L, *Biores Technol*, 250 (2018) 256.
6 Balat M, *Energy Convers Manag*, 52 (2011) 858.
7 Kozlowski J T & Davis R J, *ACS Catal*, 3 (2013) 1588.
8 Aitchison H, Wingad R L & Wass D F, *ACS Catal*, 6 (2016) 7125.
9 Ho C R, Shylesh S & Bell A T, *ACS Catal*, 6 (2016) 939.
10 (a) Wu X, Fang G, Tong Y, Jiang D, Liang Z, Leng W, Liu L, Tu P, Wang H, Ni J & Li X, *Chem Sus Chem*, 11 (2018) 71;

(b) Gabriëls D, Hernández W, Sels B, Van Der Voort P & Verberckmoes A, *Catal Sci Technol*, 5 (2015) 3876; (c) Hanspal S, The Guerbetcoupling of ethanol into butanol over calcium hydroxyapatite catalysts, Ph.DThesis, Univ. Virginia, May (2016). Z.D Young, The role of aldol condensation and hydrogen transfer reactions in the Guerbetcoupling reaction of ethanol over acid-base catalysts, Ph.D Thesis, Univ.Virginia, Aug (2017).

11 Tsuchida T, Sakuma S, Takeguchi T & Ueda W, *Ind Eng Chem Res*, 45 (2006) 8634.

12 Cimino S, Lisi L & Romanucci S, *Catalysis Today*, 304 (2018) 58.

13 Ke Wu Yang X, Jiang Z & Zhang W C, *Chinese Chem Lett*, 15 (2004) 1497.

14 (a) Riittonen T, Toukoniitty E, Madnani D K, Leino A R, Kordas K, Szabo M, Sapi A, Arve K, Wärnåand J & Mikkola J P, *Catalysts*, 2 (2012) 68; (b) Riittonen T, Ernen K, M-ki-Arvela P, Shchukarev A, Rautio A R, Kordas K, Kumar N, Salmi T & Mikkola J P, *Renewable Energy*, 74 (2015) 369.

15 Jordison T L, Lira C T & Miller D J, *Ind Eng Chem Res*, 54 (2015) 10991.

16 Sun Z, Vasconcelos A C, Bottari G, Stuart M C A, Bonura G, Cannilla C, Frusteri F & Barta K, *ACS Sustainable Chem Eng*, 5 (2017) 1738.

17 Ghaziaskar H S & Charles Xu C, *RSC Adv*, 3 (2013) 4272.

18 Pang J, Zheng M, He L, Li L, Pan X, Wang A, Wang X & Zhang T, *J Catal*, 344 (2016) 184.

19 Chistyakov A V, Zharova P A, Nikolaev S A & Tsodikov M V, *Catal Today*, 279 (2017) 124. Kinetics and Catalysis, 57 (2016) 6.

20 Quesada J, Arreola-Sánchez R, Faba L, Díaz E, Rentería-Tapia V M & Ordóñez S, *Appl Catal A Gen*, 551 (2018) 23.

21 Ni Li X, Peng S S, Feng L N, Lu S Q, Ma L J & Yue M B, *Micropor Mesopor Mater*, 261 (2018) 44.

22 Zaccheria F, Scotti N & Ravasio N, *Chem Cat Chem*, 10 (2018) 1.

23 Quesada J, Faba L, Díaz E & Ordóñez S, *Appl Catal A Gen*, 559 (2018) 167.

24 Earley J H, Bourne R A, Watson M J & Poliakoff M, *Green Chem*, 17 (2015) 3018.

25 Perronea O M, Lobefaro F, Aresta M, Nocito F, Boscolo M & Dibenedetto A, *Fuel Process Technol*, 177 (2018) 353.

26 (a) Apuzzo J, Cimino S & Lisi L, *RSC Adv*, 8 (2018) 25846. (b) Iman Nezam, Lars Peereboom & Dennis J Miller, *J Cleaner Prod*, 209 (2019) 1365.

27 Yang R, Li X, Wu J, Zhang X & Zhang Z, *J Phys Chem C*, 113 (2009) 17787.

28 Cerritos R C, Ramírez R F, Alvarado A F A, Rosales J M M & García T V, *Ind Eng Chem Res*, 50 (2011) 2576.

29 Roy P S, Park C S, Raju A S K & Kim K, *J CO_2 Utilization*, 12 (2015) 12.

30 (a) Tribalis A, Panagiotou G D, Bourikas K, Sygellou L, Kennou S, Ladas S, Lycourghiotis A & Kordulis C, *Catal*, 6 (2016) 11;(b) Sánchez-Sánchez M C, Navarro R M, *J L G Int J Hydrogen Energy*, 32 (2007) 1462. Ponminiessarry, Studies on thepreparation of supported nickel catalysts using bis(ethylene diamine) nickel(II) complexes as precursorsPh.D Thesis, Cochin University of Science and Technology, Cochin, (2010)

31 Daza C E, Gallego J, Mondragon F, Moreno S & Molina R, *Fuel*, 89 (2010) 592.

32 Debek R, Radlik M, Motak M, Galvez M E, Turek W, da Costa P & Grzybek T, *Catal Today*, 257 (2015) 59.

33 Grosvenor A P, Biesinger M C, Smart R S C & McIntyre N S, *Surf Sci*, 600 (2006) 1771.

34 (a) Bunch A Y, Wang X Q & Ozkan U S, *J Mol Catal A*, 270 (2007) 264. (b) Ding L H, Zheng Y, Zhang Z S, Ring Z & Chen J W, *J Catal*, 241 (2006) 435.

35 Practical Surface Analysis,2nd ed. Ed.D. Briggs, M.P.Seah, Auger and X-RayPhotoelectron Spectroscopy. Vol I, John Wiley, New York, (1990) 657

36 Haack L P, deVries J E, Otto K & Chattha M S, *Appl Catal A Gen*, 82 (1992) 199.

37 AIvero R, Bernai A, Carrizosa I & Odriozola J A, *Inorg Chim Acta*, 140 (1987) 45.

38 Nelson A E & Schulz K H, *Appl Surf Sci*, 210 (2003) 206.

39 Jiang L, Zhu H, Razzaq R, Zhu M, Li C & Li Z, *Int J Hydrogen Energy*, 37 (2012) 15914.

40 Murugan B, Ramaswamy A V, Srinivas D, Gopinathand C S & Ramaswamy V, *Chem Mater*, 17 (2005) 3983.

41 Pfau A & Schierbaum K D, *Surf Sci*, 321 (1994) 71.

42 Zhang F, Wang P, Koberstein J, Khalid S & Chan S W, *Surf Sci*, 563 (2004) 74.

43 Morant C, Sanz J M, Galan L, Soriano L & Rueda F, *Surf Sci*, 218 (1989) 331.

44 Briggs D, Seah, Mp. Practical surface analysis by auger and X-ray photoelectron Spectroscopy, Practical surface analysis, 2nd edn., vol I, auger and X-ray photoelectron spectroscopy. Edited by D. Briggs, M. P. Seah, John Wiley, New York, (1990), 657 pp., price: £86.50. ISBN 0471 92081 9 Chichester: Wiley; (1990).

45 Reddy B M, Ganesh I & Reddy I E P, *J Phys Chem B*, 101 (1997) 1769.

46 Garbarino G, Wang C, Valsamakis I, Chitsazan S, Riani P, Finocchio E, Fi Stephanopoulos M & Busca G, *Appl Catal B Environ*, 200 (2017) 458.

47 Vazquez A, Lopez T, Gomez R & Bokhimi X, *J Mol Catal A Chem*, 167 (2001) 91.

48 Young Z D, Hanspal S & Davis R J, *ACS Catal*, 6 (2016) 3193.

49 Marcu I C, Tanchoux N, Fajula F & Tichit D, *Catal Today*, 147 (2009) 231.

50 Jiang D, Wu X, Mao J, Ni J & Li X, *Chem Comm*, 52 (2016) 13749.

51 Benito P, Vaccari A, Antonetti C, Licursi D, Schiarioli N, Rodriguez-Castell E & Galletti A M R, *J Cleaner Prod*, 209 (2019) 1614.

52 Wang D, Liu Z & Liu Q, *RSC Adv*, 9 (2019) 18941.

53 Lopez-Olmosa C, Guerrero-Ruizb A & Rodríguez-Ramosa I, Catal Today, 357 (2020) 132.

54 Nikolaev S A, Tsodikov M V, Chistyakov A V, Zharova P A & Ezzgelenko D I, *J Catal*, 369 (2019) 501.